Supporting Information

Efficient Polysulfide Redox Enabled by Lattice–Distorted Ni_3Fe Intermetallic Electrocatalyst Modified Separator for Lithium-Sulfur Battery

Ze Zhang,[1#] A-Hu Shao,[1#] Dong-Gen Xiong,[1] Ji Yu,[1] Nikhil Koratkar,[2,3] and Zhen-Yu Yang[1*]*

[1] College of Chemistry, Key laboratory of Jiangxi Province for Environment and Energy Catalysis, Nanchang University, Nanchang, Jiangxi, 330031, China.

[2] Department of Mechanical, Aerospace and Nuclear Engineering, Rensselaer Polytechnic Institute, 110, 8th Street, Troy, NY 12180, USA.

[3] Department of Materials Science and Engineering. Rensselaer Polytechnic Institute, 110, 8th Street, Troy, NY 12180, USA.

AUTHOR INFORMATION

Corresponding Author

*E-mail: koratn@rpi.edu; zyyang@ncu.edu.cn

[#] Z. Zhang and A. Shao contributed equally to this work.

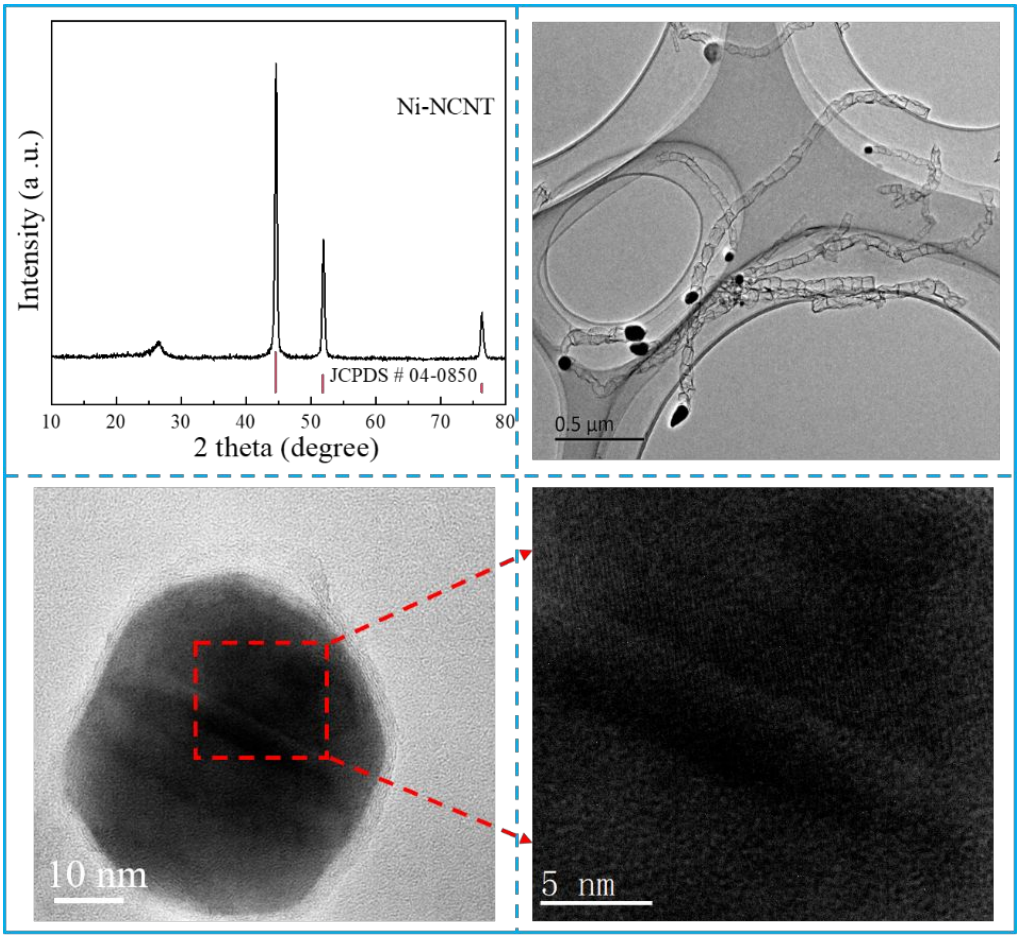

Figure S1. XRD pattern and TEM images of control sample Ni@NCNT.

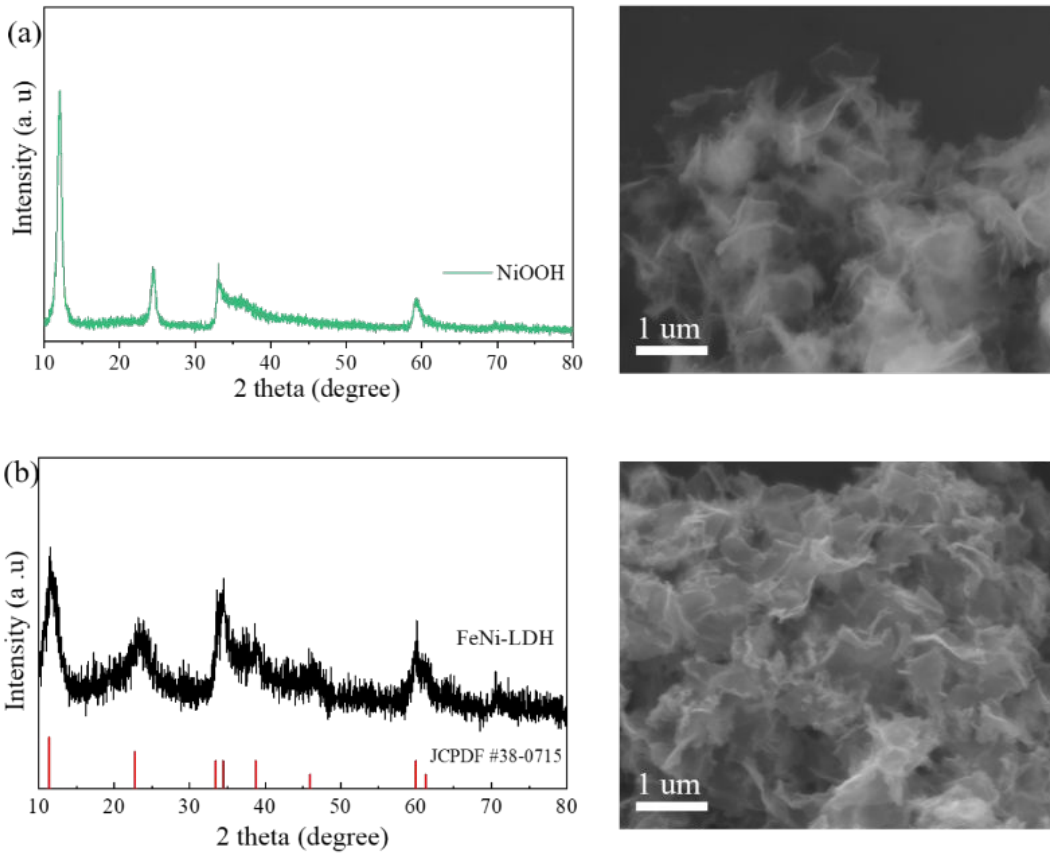

Figure S2. XRD pattern and SEM image of the different precursors: a) NiOOH, b) FeNi-LDH.

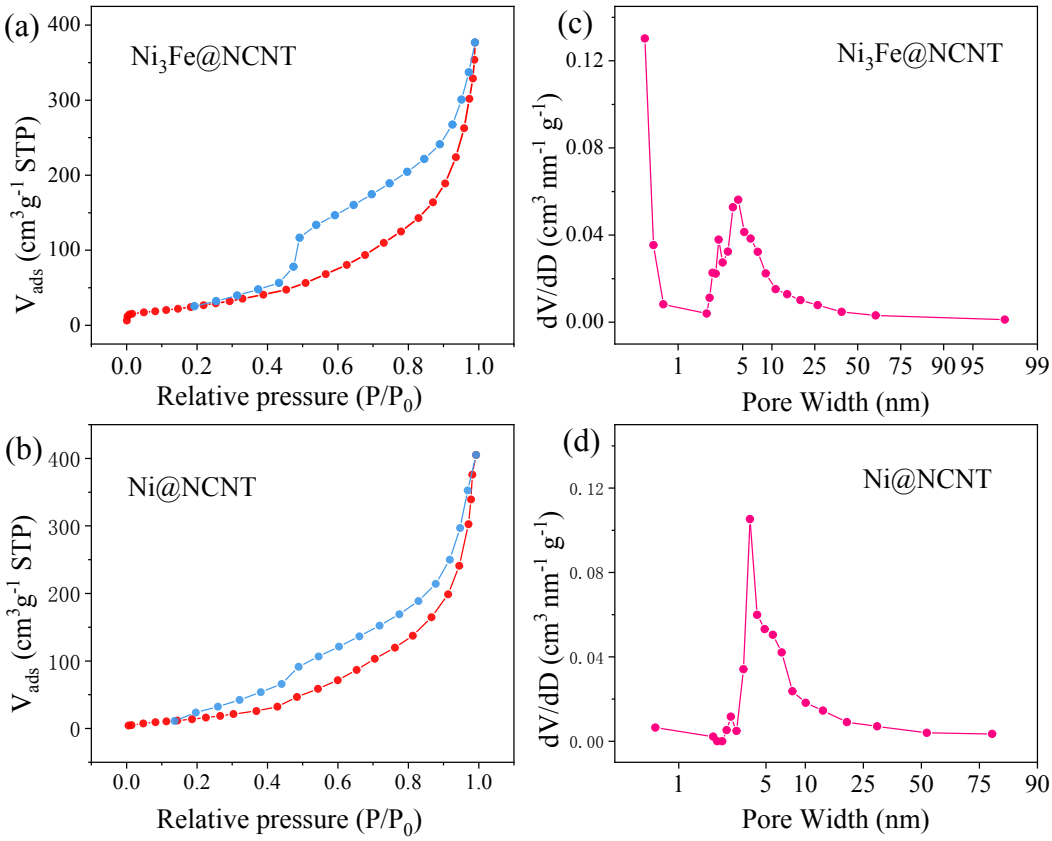

Figure S3. N_2 adsorption-desorption isotherms and pore size distribution of a-b) Ni_3Fe@NCNT and c-d) Ni@NCNT sample.

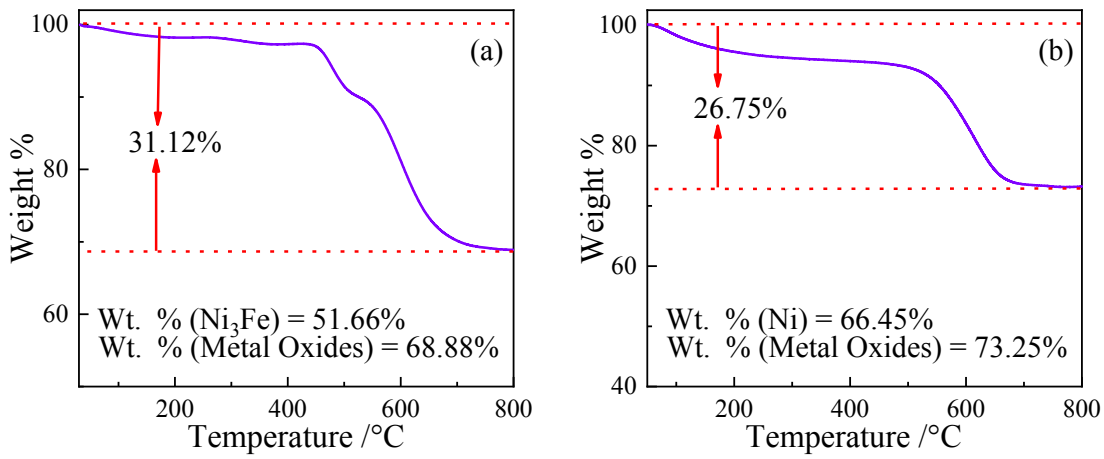

Figure S4. TGA curve of a) Ni_3Fe@NCNT, and b) Ni@NCNT samples.

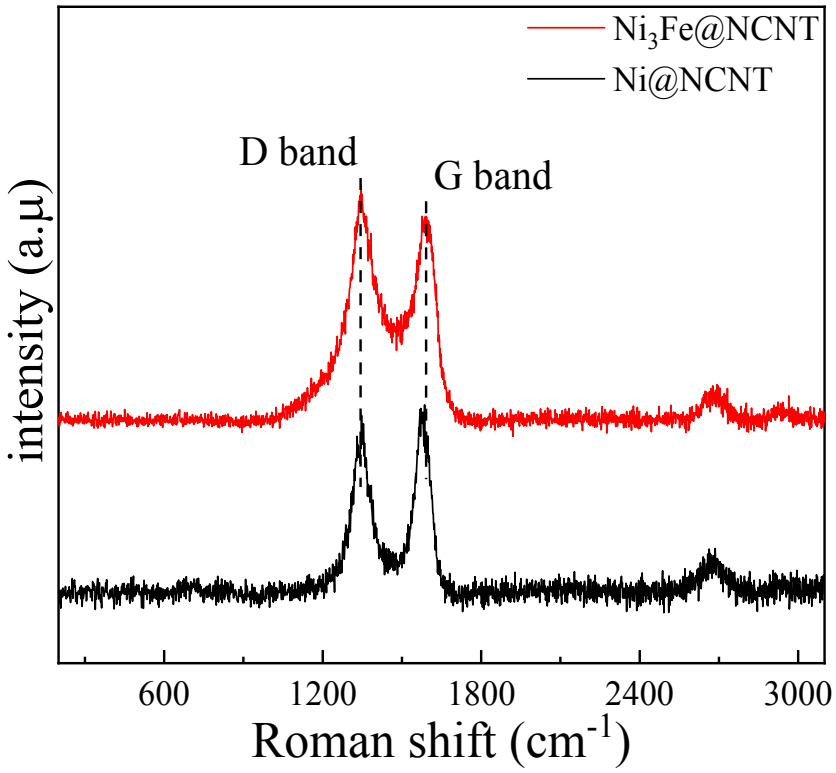

Figure S5. Raman data for the Ni_3Fe@NCNT and Ni@NCNT.

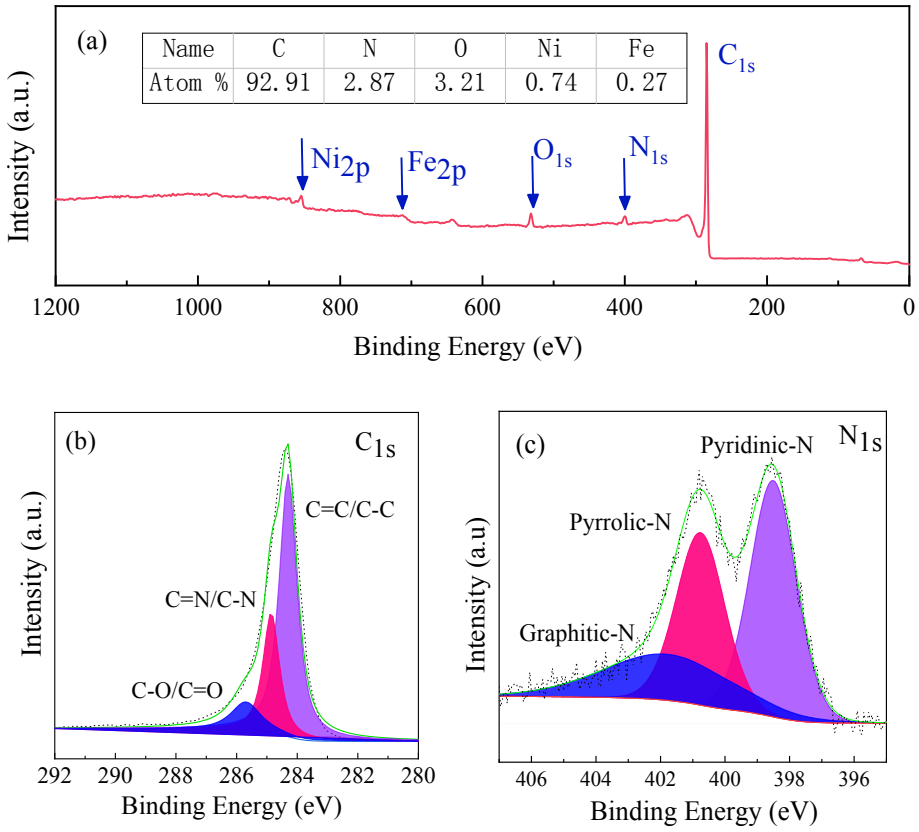
(a)
Name | C | N | O | Ni | Fe
Atom % | 92.91 | 2.87 | 3.21 | 0.74 | 0.27
C1s
Ni2p
Fe2p
O1s
N1s
Intensity (a.u.)
1200
1000
800
600
400
200
0
Binding Energy (eV)
(b)
C1s
C=C/C-C
C=N/C-N
C-O/C=O
Intensity (a.u.)
292
290
288
286
284
282
280
Binding Energy (eV)
(c)
N1s
Pyridinic-N
Pyrrolic-N
Graphitic-N
Intensity (a.u)
406
404
402
400
398
396
Binding Energy (eV)

S6

Figure S6. a) Survey XPS result, refined b) C 1s, and c) N 1s spectrum of Ni_3Fe@NCNT sample.

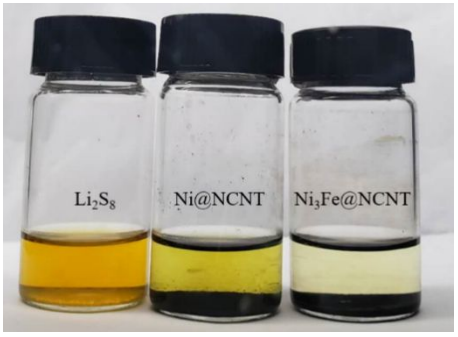

Figure S7. Static adsorption of lithium polysulfide for different sorbents.

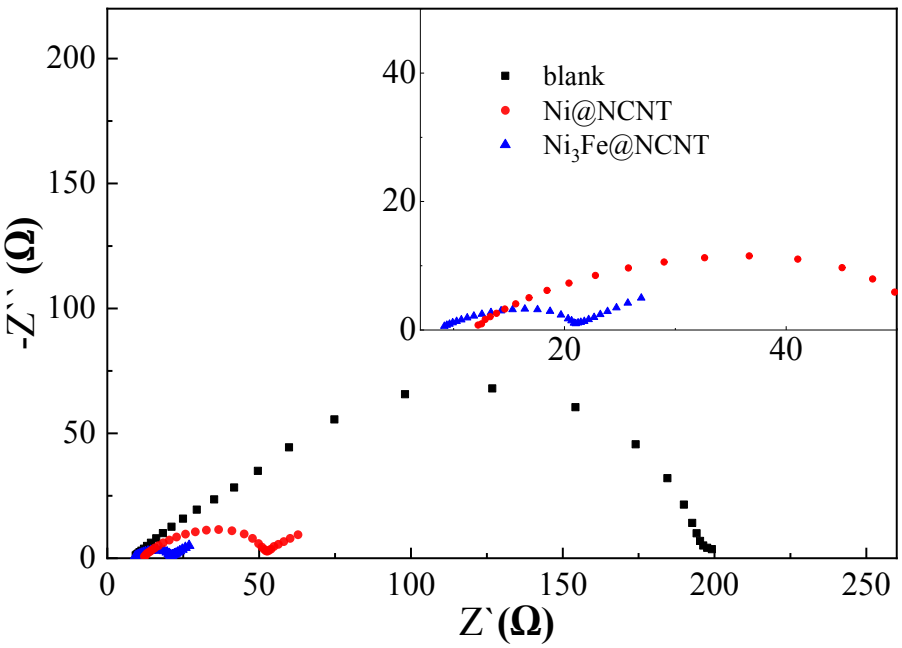

Figure S8. EIS profiles of the Li_2S_8 symmetric cells with different electrodes.

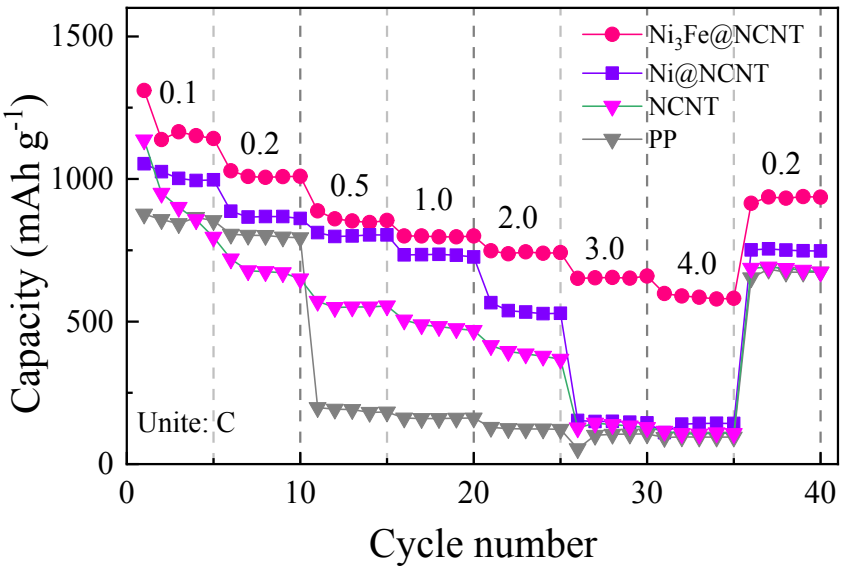

Figure S9. The rate capability of the Li-S cells employing different separators at various C-rates.

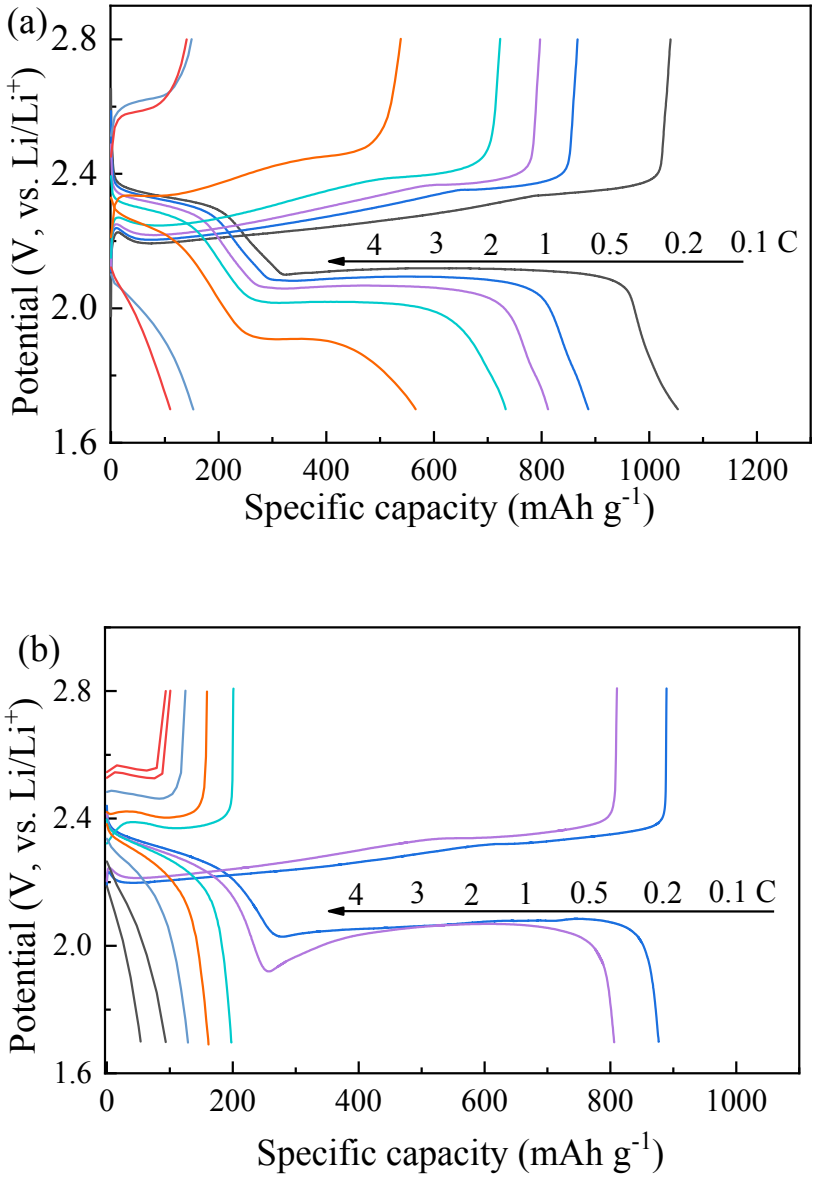

Figure S10. Discharge-charge curves of a) Ni@NCNT modified, and b) PP separator at various C-rates.

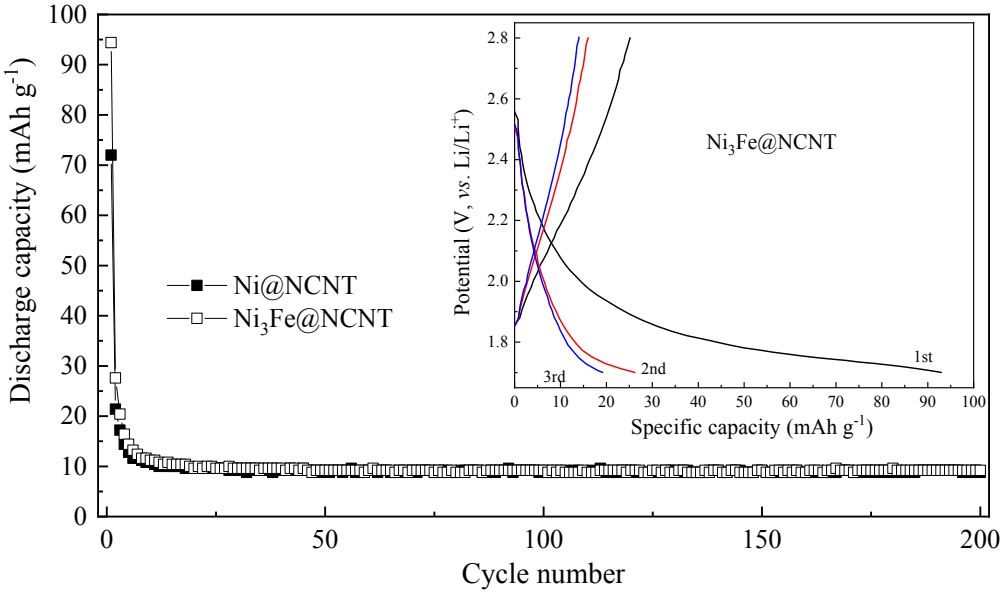

Figure S11. Cycle performance of Li/Ni_3Fe@NCNT cell and Li/Ni@NCNT cell in the potential range of 1.7-2.8 V vs. Li/Li^+. Inset shows the initial three discharge/charge curves of Li/Ni_3Fe@NCNT cell.

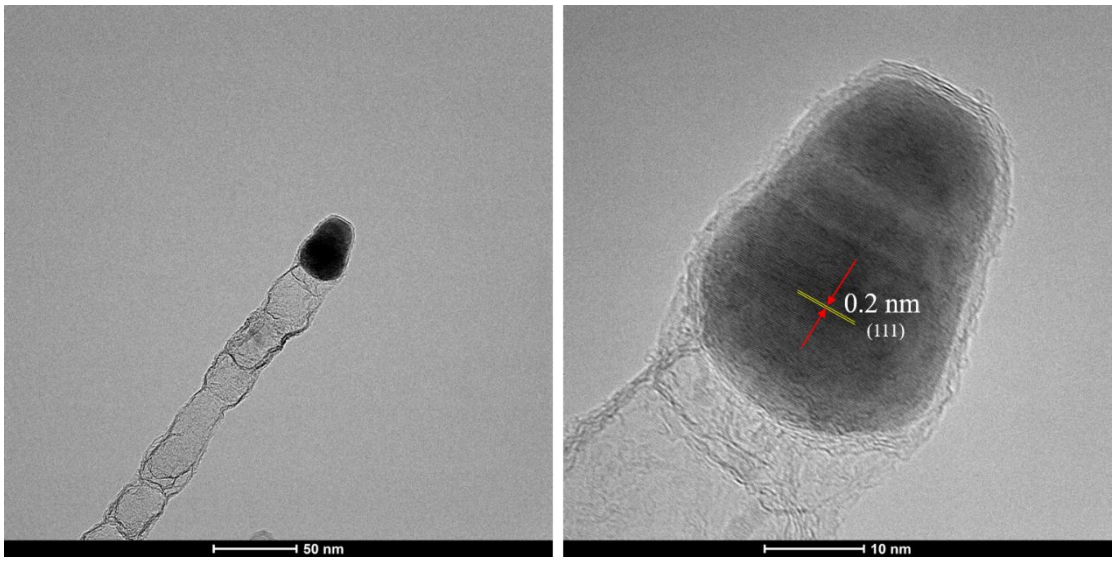

Figure S12. TEM images of Ni@NCNT sample after cycling.

Interlayer material	Sulfur content (in cathode)	Sulfur loading (mg cm^{-2})	Rate capabilityr (mAh g^{-1})	Initial capacity (mAh g^{-1})	Capacity fading rate & cycles	Ref.
Ni_3Fe@NCNT	*70%, Sulfur*	*1.6*	*4.0 C, 598*	*1.0 C, 896* *0.2 C, 1095*	*0.034%, 1000* *0.12%, 200*	*This work*
MoP_2&CNT	50%, Sulfur	1.2	5.0 C, 360	1 .0 C, 619	0.025%, 500	1
rGO@MoS_2	70%, Sulfur	1.8-2.0	2.0 C, 610	1.0 C, 877	0.116%, 500	2
Indium nitride	80%, nano S	1.5	5.0 C, 415	1.0 C, 861	0.028%, 1000	3
Prussian blue	60%, S-KB		1.0 C, 698	1.0 C, 792	0.03%, 1000	4
MXene	54.4%, S-CB	1.2	1.0 C, 744	0.5 C, 814	0.062%, 500	5
MoO_3	49%, S-CNT	0.9~1.0	1.0 C, 1074	0.5 C , 1377	0.251%, 200	6
Ni_3FeN/G	63%, S-CNT	1.2	3.0 C, 822	1.0 C, 1060	0.12%, 180	7

Graphene/PP/ Al_2O_3	60%, S-KB	0.75	2.0 C, 780	0.2 C, 1068	0.25%, 100	8
Pd_3Co/MWCNT	60% , Sulfur	1.0	2.0 C, 953	2.0 C, 953	0.07% , 300	9
Single Co catalyst	63%, S-CNT	1.2	3.0 C, 800	0.5 C, 1130	0.086%, 300	10

Table S1 Electrochemical performance comparison of Li-S cells based on Ni_3Fe@NCNT catalytic separator and other similar materials in recent works.

Reference

1 Luo, Y.; Luo, N.; Kong, W.; Wu, H.; Wang, K.; Fan, S.; Duan, W.; Wang, J. Multifunctional Interlayer Based on Molybdenum Diphosphide Catalyst and Carbon Nanotube Film for Lithium–Sulfur Batteries. *Small* **2018,** *14*, 1702853.

2 Tan, L.; Li, X.; Wang, Z.; Guo, H.; Wang, J. Lightweight Reduced Graphene Oxide@MoS2 Interlayer as Polysulfide Barrier for High-Performance Lithium–Sulfur Batteries. *ACS Appl. Mater. Interfaces* **2018,** *10*, 3707-3713.

3. Zhang, L.; Chen, X.; Wan, F.; Niu, Z.; Wang, Y.; Zhang, Q.; Chen, J. Enhanced Electrochemical Kinetics and Polysulfide Traps of Indium Nitride for Highly Stable Lithium–Sulfur Batteries. *ACS Nano* **2018,** *12*, 9578-9586.

4. Wu, X.; Fan, L.; Qiu, Y.; Wang, M.; Cheng, J.; Guan, B.; Guo, Z.; Zhang, N.; Sun, K. Ion-Selective Prussian-Blue-Modified Celgard Separator for High-Performance Lithium-Sulfur Battery. *ChemSusChem* **2018,** *11*, 3345-3351.

5. Song, J.; Su, D.; Xie, X.; Guo, X.; Bao, W.; Shao, G.; Wang, G. Immobilizing Polysulfides with MXene-Functionalized Separators for Stable Lithium–Sulfur Batteries. *ACS Appl. Mater. Interfaces* **2016,** *8*, 29427-29433.

6. Imtiaz, S.; Ali Zafar, Z.; Razaq, R.; Sun, D.; Xin, Y.; Li, Q.; Zhang, Z.; Zheng, L.; Huang, Y.; Anderson, J. A. Electrocatalysis on Separator Modified by Molybdenum Trioxide Nanobelts for Lithium–Sulfur Batteries. *Adv. Mater. Interfaces* **2018,** *5*, 1800243.

7. M. Zhao, H. J. Peng, Z. W. Zhang, B. Q. Li, X. Chen, J. Xie, X. Chen, J. Y. Wei, Q. Zhang, J. Q. Huang, *Angew. Chem.*, **2019**, *131*, 3819-3823.

8. Zhao, M.; Peng, H. J.; Zhang, Z. W.; Li, B. Q.; Chen, X.; Xie, J.; Chen, X.; Wei, J. Y.; Zhang, Q.; Huang, J. Q. Activating Inert Metallic Compounds for High-Rate Lithium–Sulfur Batteries Through in Situ Etching of Extrinsic Metal. *Angew. Chem.* **2019,** *131*, 3819-3823.

9. Cho, S. H.; Cho, S. M.; Bae, K. Y.; Kim, B. H.; Son, B. D.; Yoon, W. Y. Improving Electrochemical Properties of Lithium–Sulfur Batteries by Adding A Catalyst-Embedded Interlayer. *Electrochim. Acta* **2019,** *315*, 33-40.

10. Xie, J.; Li, B.-Q.; Peng, H.-J.; Song, Y.-W.; Zhao, M.; Chen, X.; Zhang, Q.; Huang, J.-Q. Implanting Atomic Cobalt within Mesoporous Carbon toward Highly Stable Lithium–Sulfur Batteries. *Adv. Mater.* **2019,** *31*, 1903813.